JOURNAL OF GUIDANCE, CONTROL, AND DYNAMICS
Vol. 27, No. 2, March–April 2004

Singularity Analysis and Visualization for Single-Gimbal Control Moment Gyro Systems

Bong Wie*
Arizona State University, Tempe, Arizona 85287-6106

The singularity problem inherent in redundant single-gimbal control moment gyro (CMG) systems is examined. It is intended to provide a comprehensive mathematical treatment of the CMG singularity problem, expanding upon the previous work by Margulies, Aubrun, and Bedrossian. However, particular emphasis is placed on characterizing and visualizing the physical as well as mathematical nature of the singularities, singular gimbal angles, singular momentum surfaces, null motion manifolds, and degenerate null motions. The mathematical framework for characterizing the geometric property of singular surfaces is also established by applying the surface theory of differential geometry. Two and three parallel single-gimbal CMG configurations and a typical pyramid array of four single-gimbal CMGs (including a special case of 90-deg skew angle) are examined in detail to illustrate the various concepts and approaches useful for characterizing and visualizing the CMG singularities.

I. Introduction

CONTROL moment gyros (CMGs), as applied to spacecraft attitude control and momentum management, have been extensively studied in the past[1–7] and more recently in Refs. 8–16. They have been successfully employed mainly for large space vehicles, such as the Skylab, the MIR space station, and the International Space Station (ISS). However, CMGs have never been used in commercial satellites because their higher torque capabilities are not needed by most commercial satellites and also because CMGs are much more expensive and mechanically complex than reaction wheels.

A CMG contains a spinning rotor with large, constant angular momentum, but whose angular momentum vector direction can be changed with respect to the spacecraft by gimballing the spinning rotor. The spinning rotor is mounted on a gimbal (or a set of gimbals), and torquing the gimbal results in a precessional, gyroscopic reaction torque orthogonal to both the rotor spin and gimbal axes. The CMG is a torque amplification device because small gimbal torque input produces large control torque output on the spacecraft. Because the CMGs are capable of generating large control torques and storing large angular momentum over long periods of time, they have been employed for attitude control and momentum management of large space vehicles such as the ISS. Four parallel-mounted double-gimbal CMGs with a total weight of about 2400 lb and with a design life of 10 years are employed on the ISS.

The next-generation Earth imaging satellites, such as the Pleiades high-resolution imaging satellite, will require rapid rotational maneuverability (e.g., a slew rate of 4 deg/s) for high-resolution images. Rather than sweep a gimbaled imaging system from side to side, the whole spacecraft body will turn rapidly. Pointing the entire spacecraft body allows the body-fixed imaging system to achieve a higher definition and improves the resolution for its images. Because the overall cost and effectiveness of such agile imaging satellites are greatly affected by the average retargeting time, the development of an agile attitude control system employing CMGs is of current practical interest.[17–21] For example, the Pleiades high-resolution imaging satellite will be controlled by a pyramid cluster of four single-gimbal CMGs (Astrium's CMG 15-45S), and it will be able to perform a 60-deg crosstrack slew manuever in less than 25 s.[17–20]

Received 1 August 2002; revision received 24 April 2003; accepted for publication 26 August 2003.

*Professor, Department of Mechanical and Aerospace Engineering; bong.wie@asu.edu. Associate Fellow AIAA.

However, the use of CMGs necessitates the development of CMG steering logic, which generates the CMG gimbal rate commands for the commanded spacecraft control torques. One of the principal difficulties in using CMGs for spacecraft attitude control and momentum management is the well-known geometric singularity problem in which no control torque is generated for the commanded control torque along a certain direction. At such a singularity, CMG torque is available in all but one particular direction, called the singular direction.

As evidenced in Refs. 1–21, most CMG researchers have been focusing on the development of singularity-avoidance steering logic. However, this paper focuses on the singularity problem itself and is intended to provide its coherent, comprehensive mathematical treatment. This paper is also intended to provide the reader with a summary of various approaches with many illustrative examples with significant new results. In particular, this paper will provide the comprehensive mathematical framework to CMG researchers with a renewed practical interest in developing an agile attitude control system employing smaller CMGs for small agile satellites.[17–21]

The remainder of this paper is outlined as follows. In Sec. II, a summary of various single-gimbal CMG systems will be presented. Such CMG systems will be used throughout the paper to illustrate the various concepts and approaches useful for characterizing and visualizing the CMG singularities. In Sec. III, the singular momentum surfaces will be characterized and visualized using a method introduced by Margulies and Aubrun.[2] Several illustrative examples with significant new results will be presented. Section IV will describe a new approach for analyzing the CMG singularity problem. This new method is based on the Binet–Cauchy identity. Its practicality in being applied to a pyramid array of four single-gimbal CMGs will be demonstrated. In Sec. V, the CMG null motion problem will be examined, expanding upon the previous work of Bedrossian et al.[4,5] In particular, the degenerate null motion will be examined in detail and several illustrative examples with significant new results will be presented. In Sec. VI, the singularity surface problem will be examined by applying the surface theory of differential geometry. However, this section is intended to provide the reader with the basic mathematical foundation of the theory of differential geometry as applied to the CMG systems. Although a further study is needed to fully demonstrate its practicality, this section on the surface theory of differential geometry will certainly help the reader further advance the subject matter.

II. Single-Gimbal CMG Systems

This section provides a summary of a few representative single-gimbal CMG systems. These CMG systems will be used as illustrative examples throughout the paper to illustrate the various concepts

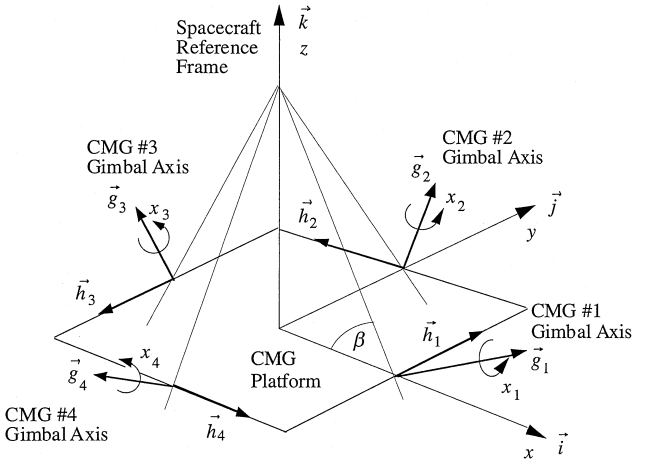

Fig. 1 Pyramid mounting arrangement of four single-gimbal CMGs.

and approaches useful for characterizing and visualizing the CMG singularities.

Pyramid Array of Four Single-Gimbal CMGs

A typical pyramid array of four single-gimbal CMGs is illustrated in Fig. 1. The total angular momentum vector of four single-gimbal CMGs, $\boldsymbol{H}$, is simply given by

$$\boldsymbol{H} = \boldsymbol{h}_1 + \boldsymbol{h}_2 + \boldsymbol{h}_3 + \boldsymbol{h}_4 \tag{1}$$

where $\boldsymbol{h}_i$ is the angular momentum vector of the ith CMG and it is assumed that $|\boldsymbol{h}_i| = 1$ without loss of generality. The ith gimbal angle, x_i, describes rotation of $\boldsymbol{h}_i$ about the normalized gimbal-axis vector, $\boldsymbol{g}_i$ ($|\boldsymbol{g}_i| = 1$); that is, $\boldsymbol{g}_i \cdot \boldsymbol{h}_i = 0$ and $\boldsymbol{h}_i = \boldsymbol{h}_i(x_i)$.

For the pyramid mount of four single-gimbal CMGs with skew angle of β as illustrated in Fig. 1, the gimbal-axis vectors can be simply represented as $\boldsymbol{g}_1 = \sin\beta\boldsymbol{i} + \cos\beta\boldsymbol{k}$, $\boldsymbol{g}_2 = \sin\beta\boldsymbol{j} + \cos\beta\boldsymbol{k}$, $\boldsymbol{g}_3 = -\sin\beta\boldsymbol{i} + \cos\beta\boldsymbol{k}$, and $\boldsymbol{g}_4 = -\sin\beta\boldsymbol{j} + \cos\beta\boldsymbol{k}$.

The total CMG momentum vector $\boldsymbol{H}$ is often expressed in a spacecraft reference frame (x, y, z) with a set of orthogonal unit vectors $\{\boldsymbol{i}, \boldsymbol{j}, \boldsymbol{k}\}$ as follows:

$$\begin{aligned}\boldsymbol{H} &= H_x\boldsymbol{i} + H_y\boldsymbol{j} + H_z\boldsymbol{k} \\ &= [\,\boldsymbol{i} \quad \boldsymbol{j} \quad \boldsymbol{k}\,]\begin{bmatrix} H_x \\ H_y \\ H_z \end{bmatrix} = [\,\boldsymbol{i} \quad \boldsymbol{j} \quad \boldsymbol{k}\,]\mathbf{H}\end{aligned} \tag{2}$$

where $\mathbf{H} = (H_x, H_y, H_z) \equiv [H_x \;\; H_y \;\; H_z]^T$ is the representation of the vector $\boldsymbol{H}$ with respect to the basis vectors $\{\boldsymbol{i}, \boldsymbol{j}, \boldsymbol{k}\}$. Although the column vector $\mathbf{H}$ should be distinguished from the vector $\boldsymbol{H}$ itself, it is often called a vector. However, the meaning should be clear from the context and in general we must be clear on what is meant by a vector.

For the pyramid mount of four single-gimbal CMGs with skew angle of β, the total CMG momentum vector can be represented in matrix form as

$$\begin{aligned}\mathbf{H} &= \mathbf{h}_1(x_1) + \mathbf{h}_2(x_2) + \mathbf{h}_3(x_3) + \mathbf{h}_4(x_4) \\ &= \begin{bmatrix} -c\beta\sin x_1 \\ \cos x_1 \\ s\beta\sin x_1 \end{bmatrix} + \begin{bmatrix} -\cos x_2 \\ -c\beta\sin x_2 \\ s\beta\sin x_2 \end{bmatrix} \\ &\quad + \begin{bmatrix} c\beta\sin x_3 \\ -\cos x_3 \\ s\beta\sin x_3 \end{bmatrix} + \begin{bmatrix} \cos x_4 \\ c\beta\sin x_4 \\ s\beta\sin x_4 \end{bmatrix}\end{aligned} \tag{3}$$

where $c\beta \equiv \cos\beta$, $s\beta \equiv \sin\beta$. Note that $\mathbf{h}_i$ are periodic with a period of 2π and that

$$\frac{d^2\mathbf{h}_i}{dx_i^2} = -\mathbf{h}_i \tag{4}$$

The differential of $\mathbf{H}$ becomes

$$\begin{aligned}d\mathbf{H} &= \mathbf{f}_1\,\mathrm{d}x_1 + \mathbf{f}_2\,\mathrm{d}x_2 + \mathbf{f}_3\,\mathrm{d}x_3 + \mathbf{f}_4\,\mathrm{d}x_4 \\ &= \mathbf{A}\,\mathrm{d}\mathbf{x}\end{aligned} \tag{5}$$

where $\mathrm{d}\mathbf{x} = (\mathrm{d}x_1,\ \mathrm{d}x_2,\ \mathrm{d}x_3,\ \mathrm{d}x_4)$, and $\mathbf{A}$ is the Jacobian matrix defined as

$$\begin{aligned}\mathbf{A} &= \begin{bmatrix} \mathbf{f}_1 & \mathbf{f}_2 & \mathbf{f}_3 & \mathbf{f}_4 \end{bmatrix} \\ &= \begin{bmatrix} -c\beta\cos x_1 & \sin x_2 & c\beta\cos x_3 & -\sin x_4 \\ -\sin x_1 & -c\beta\cos x_2 & \sin x_3 & c\beta\cos x_4 \\ s\beta\cos x_1 & s\beta\cos x_2 & s\beta\cos x_3 & s\beta\cos x_4 \end{bmatrix}\end{aligned} \tag{6}$$

Equation (5) represents a linear mapping from $\mathrm{d}\mathbf{x} = (\mathrm{d}x_1, \mathrm{d}x_2, \mathrm{d}x_3, \mathrm{d}x_4)$ to $\mathrm{d}\mathbf{H} = (\mathrm{d}H_x, \mathrm{d}H_y, \mathrm{d}H_z)$. Consequently, we obtain

$$\dot{\mathbf{H}} = \mathbf{A}\dot{\mathbf{x}} \tag{7}$$

where $\dot{\mathbf{H}} = \mathrm{d}\mathbf{H}/\mathrm{d}t$ and $\dot{\mathbf{x}} = \mathrm{d}\mathbf{x}/\mathrm{d}t$.

2-SPEED Single-Gimbal CMG System[1]

A special case with $\beta = \pi/2$ was employed by Crenshaw for the so-called 2-SPEED (Two Scissored Pair Ensemble, Explicit Distribution) single-gimbal CMG control system.[1] For this configuration, we simply have two orthogonal pairs of two parallel single-gimbal CMGs with a Jacobian matrix of the form

$$\mathbf{A} = \begin{bmatrix} 0 & \sin x_2 & 0 & -\sin x_4 \\ -\sin x_1 & 0 & \sin x_3 & 0 \\ \cos x_1 & \cos x_2 & \cos x_3 & \cos x_4 \end{bmatrix} \tag{8}$$

This special configuration is also of practical importance. Many other CMG configurations are in fact some variant of this basic arrangement of two orthogonal pairs of two parallel CMGs, known as the 2-SPEED CMG system in the literature.

Two and Three Parallel Single-Gimbal CMG Configurations

Two and three single-gimbal CMG configurations with parallel gimbal axes have also been studied for two-axis control applications.[1,2] Consider first a case with only two CMGs without redundancy. The momentum vectors $\boldsymbol{H}_1$ and $\boldsymbol{H}_2$ move in the (x, y) plane normal to the gimbal axis, as shown in Fig. 2. For such scissored single-gimbal CMGs, the total CMG momentum vector can be represented in matrix form as

$$\mathbf{H} = \begin{bmatrix} \cos x_1 + \cos x_2 \\ \sin x_1 + \sin x_2 \end{bmatrix} \tag{9}$$

where a constant unit momentum for each CMG is assumed.

Defining a new set of gimbal angles (α, β) as

$$\alpha = (x_1 + x_2)/2, \qquad \beta = (x_2 - x_1)/2 \tag{10}$$

where α is called the rotation angle and β the scissor angle,[1] we can express the CMG momentum vector as

$$\mathbf{H} = 2\begin{bmatrix} \cos\alpha\cos\beta \\ \sin\alpha\cos\beta \end{bmatrix} \tag{11}$$

and we have

$$\dot{\mathbf{H}} = \mathbf{A}\dot{\mathbf{x}} \tag{12}$$

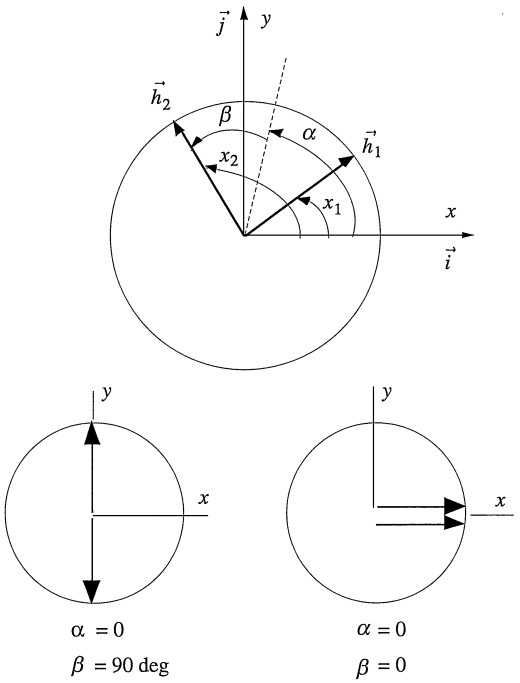

a) 0H antiparallel singularity b) 2H parallel singularity

Fig. 2 Two single-gimbal CMGs with parallel gimbal axes.[1] This CMG system remains singular for any α motion when $\beta = 0$ or 90 deg.

where $\dot{\mathbf{H}} = (\dot{H}_x, \dot{H}_y)$, $\dot{\mathbf{x}} = (\dot{\alpha}, \dot{\beta})$, and $\mathbf{A}$ is the Jacobian matrix defined as

$$\mathbf{A} = 2\begin{bmatrix} -\sin\alpha\cos\beta & -\cos\alpha\sin\beta \\ \cos\alpha\cos\beta & -\sin\alpha\sin\beta \end{bmatrix} \tag{13}$$

For a system of three single-gimbal CMGs with parallel gimbal axes, the total CMG angular momentum vector is given by

$$\mathbf{H} = \begin{bmatrix} \cos x_1 + \cos x_2 + \cos x_3 \\ \sin x_1 + \sin x_2 + \sin x_3 \end{bmatrix} \tag{14}$$

and the Jacobian matrix for $\mathbf{x} = (x_1, x_2, x_3)$ is

$$\mathbf{A} = \begin{bmatrix} -\sin x_1 & -\sin x_2 & -\sin x_3 \\ \cos x_1 & \cos x_2 & \cos x_3 \end{bmatrix} \tag{15}$$

The various CMG systems described in this section will be used throughout the paper to illustrate the various concepts and approaches discussed in this paper.

III. Singularities and Singular Surfaces

This section briefly introduces a method developed by Margulies and Aubrun[2] for analyzing and visualizing the singular momentum surfaces. Illustrative examples are presented with significant new results.

Similar to $\boldsymbol{H}$ expressed as in Eq. (2), an arbitrary vector $\boldsymbol{u}$ can also be represented as

$$\begin{aligned} \boldsymbol{u} &= u_x\boldsymbol{i} + u_y\boldsymbol{j} + u_z\boldsymbol{k} \\ &= [\,\boldsymbol{i} \quad \boldsymbol{j} \quad \boldsymbol{k}\,]\begin{bmatrix} u_x \\ u_y \\ u_z \end{bmatrix} = [\,\boldsymbol{i} \quad \boldsymbol{j} \quad \boldsymbol{k}\,]\mathbf{u} \end{aligned} \tag{16}$$

where $\mathbf{u} = (u_x, u_y, u_z) \equiv [u_x \;\; u_y \;\; u_z]^T$.

As introduced by Margulies and Aubrun,[2] let $\boldsymbol{u}$ be a unit vector of the punctured unit sphere defined as

$$\mathcal{S} = \{\boldsymbol{u} : |\boldsymbol{u}| = 1, \boldsymbol{u} \neq \pm\boldsymbol{g}_i, i = 1, \ldots, n\}$$

where $\boldsymbol{g}_i$ is the gimbal-axis vector ($|\boldsymbol{g}_i| = 1$). Such a unit vector along all possible directions in three-dimensional space (except along the gimbal-axis directions) can be parameterized as

$$\begin{aligned} \boldsymbol{u} &= u_x\boldsymbol{i} + u_y\boldsymbol{j} + u_z\boldsymbol{k} \\ &= \sin\theta_2\boldsymbol{i} - \sin\theta_1\cos\theta_2\boldsymbol{j} + \cos\theta_1\cos\theta_2\boldsymbol{k} \end{aligned} \tag{17}$$

where θ_1 and θ_2 are the rotation angles of two successive rotations about the x and y axes. The longitude and latitude angles of spherical coordinates, commonly used for a unit vector description along all possible directions in three-dimensional space, was found to be numerically ill suited for visualization of the singular surfaces. [Note that such a specific representation of $\boldsymbol{u}$ as Eq. (17) was not provided in Ref. 2.]

For a system of n single-gimbal CMGs, the differential of the total CMG momentum vector becomes

$$d\boldsymbol{H} = \sum_{i=1}^{n} \mathrm{d}\boldsymbol{h}_i = \sum_{i=1}^{n} \frac{d\boldsymbol{h}_i}{dx_i}\,\mathrm{d}x_i = \sum_{i=1}^{n} \boldsymbol{f}_i\,\mathrm{d}x_i \tag{18}$$

where $\boldsymbol{f}_i$ are unit tangent vectors defined as

$$\boldsymbol{f}_i = \boldsymbol{f}_i(x_i) = \frac{d\boldsymbol{h}_i}{dx_i} = \boldsymbol{g}_i \times \boldsymbol{h}_i \tag{19}$$

Note that $d\boldsymbol{H}$ and $\boldsymbol{f}_i$ are the equivalent vector representations of $d\mathbf{H}$ and $\mathbf{f}_i$, respectively, used in Eq. (5). The three vectors, $\{\boldsymbol{f}_i, \boldsymbol{g}_i, \boldsymbol{h}_i\}$, form a set of orthogonal unit vectors rotating about each gimbal axis $\boldsymbol{g}_i$. This set of orthonormal vectors plays a major role in developing the geometric theory of redundant single-gimbal CMGs.[2]

The $3 \times n$ Jacobian matrix $\mathbf{A}$, introduced in the preceding section, has maximum rank of 3. When the gimbal axes are not arranged to be coplanar, the minimum rank of $\mathbf{A}$ is 2. However, when $\mathrm{rank}(\mathbf{A}) = 2$, all $\boldsymbol{f}_i$ become coplanar and there exists a unit vector $\boldsymbol{u}$ normal to that plane; that is,

$$\boldsymbol{f}_i(x_i) \cdot \boldsymbol{u} \equiv \mathbf{f}_i^T\mathbf{u} = 0, \qquad i = 1, \ldots, n \tag{20}$$

Consequently, for such a case, we have

$$d\boldsymbol{H} \cdot \boldsymbol{u} = 0 \tag{21}$$

and the CMG array cannot produce any momentum vector change (or torque) along the direction of $\boldsymbol{u}$ regardless of the gimbal rates. Such a unit vector $\boldsymbol{u}$ is called the *singular vector*, and a set of gimbal angles when $\mathrm{rank}(\mathbf{A}) = 2$ is called the *singular gimbal angles*.

Because $\boldsymbol{f}_i$ is also orthogonal to $\boldsymbol{g}_i$ and $|\boldsymbol{f}_i| = 1$, singularity condition (20) can be rewritten as

$$\boldsymbol{f}_i = \pm\frac{\boldsymbol{g}_i \times \boldsymbol{u}}{|\boldsymbol{g}_i \times \boldsymbol{u}|} \tag{22}$$

Since $\boldsymbol{h}_i = \boldsymbol{f}_i \times \boldsymbol{g}_i$, the singularity condition for $\boldsymbol{h}_i(x_i)$ can also be written as

$$\boldsymbol{h}_i = \pm\frac{(\boldsymbol{g}_i \times \boldsymbol{u}) \times \boldsymbol{g}_i}{|\boldsymbol{g}_i \times \boldsymbol{u}|} \tag{23}$$

which leads to the following inner product of $\boldsymbol{h}_i$ and $\boldsymbol{u}$:

$$e_i = \boldsymbol{h}_i \cdot \boldsymbol{u} = \pm|\boldsymbol{g}_i \times \boldsymbol{u}| \equiv \pm\sqrt{1 - (\boldsymbol{g}_i \cdot \boldsymbol{u})^2} \tag{24}$$

The *singular momentum vector*, corresponding to the singular vector $\boldsymbol{u}$ and the singular gimbal angles $\mathbf{x}$, is expressed as

$$\begin{aligned} \boldsymbol{H} &= \boldsymbol{H}(\mathbf{x}(\boldsymbol{u})) = \boldsymbol{H}(\boldsymbol{u}) \\ &= \sum_i \frac{1}{e_i}(\boldsymbol{g}_i \times \boldsymbol{u}) \times \boldsymbol{g}_i \\ &= \sum_i \frac{\epsilon_i[\boldsymbol{u} - \boldsymbol{g}_i(\boldsymbol{g}_i \cdot \boldsymbol{u})]}{\sqrt{1 - (\boldsymbol{g}_i \cdot \boldsymbol{u})^2}} \end{aligned} \tag{25}$$

where $\epsilon_i = \text{sign}(e_i) = \text{sign}(\boldsymbol{h}_i \cdot \boldsymbol{u}) = \pm 1$. Note that there are 2^n combinations of ϵ_i for a clutser of n CMGs. See Ref. 2 for a detailed discussion of these 2^n combinations.

Because $\boldsymbol{u} = \boldsymbol{u}(\theta_1, \theta_2)$, we have $\boldsymbol{H} = \boldsymbol{H}(\theta_1, \theta_2)$; that is, $\boldsymbol{H}$ is also parameterized by θ_1 and θ_2. Singular momentum surfaces can be directly obtained using Eq. (25) without recourse to singular gimbal angles.

Example 3.1: Two Single-Gimbal CMGs

The singular momentum vector of the two single-gimbal CMGs with parallel gimbal axes (see Fig. 2) is given by

$$\begin{aligned} \boldsymbol{H} &= \sum_{i=1}^{2} \frac{1}{e_i} (\boldsymbol{g}_i \times \boldsymbol{u}) \times \boldsymbol{g}_i \\ &= \epsilon_1 \boldsymbol{u} + \epsilon_2 \boldsymbol{u} = 0 \quad \text{or} \quad \pm 2\boldsymbol{u} \end{aligned} \tag{26}$$

The singular momentum vector is then described as

$$\begin{aligned} \boldsymbol{H} &= H_x \boldsymbol{i} + H_y \boldsymbol{j} \\ &= \pm 2\boldsymbol{u} = \pm 2(\cos\theta \boldsymbol{i} + \sin\theta \boldsymbol{j}), \qquad 0 \le \theta \le 2\pi \end{aligned}$$

or

$$H_x^2 + H_y^2 = 4 \tag{27}$$

which represents a circle on the (H_x, H_y) plane.

Example 3.2: 2-SPEED CMG System

Consider a special case ($\beta = 90$ deg) of the pyramid configuration of four single-gimbal CMGs, called a 2-SPEED system by Crenshaw.[1] For two such orthogonal pairs of two parallel single-gimbal CMGs, the gimbal-axis vectors are simply represented by $\boldsymbol{g}_1 = \boldsymbol{i}, \boldsymbol{g}_2 = \boldsymbol{j}, \boldsymbol{g}_3 = -\boldsymbol{i}$, and $\boldsymbol{g}_4 = -\boldsymbol{j}$.

We then obtain the singular momentum vector, for all positive ϵ_i, as

$$\boldsymbol{H} = \boldsymbol{H}(\theta_1, \theta_2) = \frac{2(u_y \boldsymbol{j} + u_z \boldsymbol{k})}{\sqrt{u_y^2 + u_z^2}} + \frac{2(u_x \boldsymbol{i} + u_z \boldsymbol{k})}{\sqrt{u_x^2 + u_z^2}} \tag{28}$$

where $u_x = \sin\theta_2$, $u_y = -\sin\theta_1 \cos\theta_2$, and $u_z = \cos\theta_1 \cos\theta_2$. The so-called 4H momentum saturation singularity surface for this case when all four ϵ_i are positive can then be obtained as shown in Fig. 3.

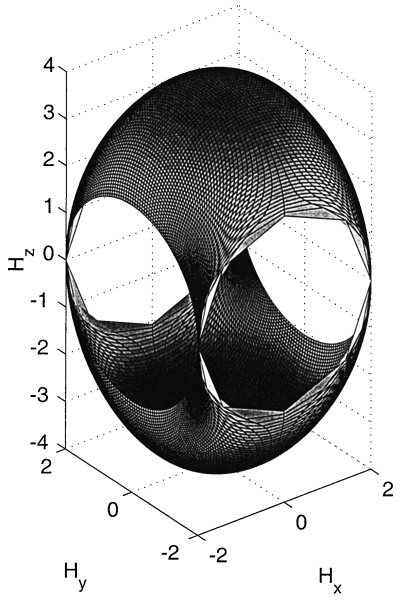

Fig. 3 Momentum saturation surface (4H singularity surface) of the 2-SPEED system of four single-gimbal CMGs ($\beta = 90$ deg). The complete momentum envelope consists of the 4H singularity surface and the four circular flat "windows" (2H singularity surface).

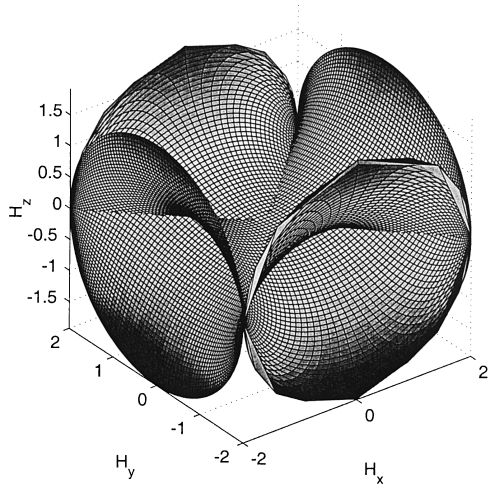

Fig. 4 Internal 0H singularity surface of the 2-SPEED system of four single-gimbal CMGs ($\beta = 90$ deg).

Note that the 4H saturation singularity surface itself does not cover the complete momentum envelope and that it has four circular holes caused by the four conditions $\boldsymbol{u} \ne \boldsymbol{g}_i$ $(i = 1, \ldots, 4)$.

A special case when two e_i are zero and the other two e_i are $+1$ produces a circular flat "window" matched with a circular hole, shown in Fig. 3. There are four circular flat windows, which are in fact the 2H singularity surfaces. The 4H saturation surface and the four circular flat windows provide the complete momentum envelope (workspace). There are also 2H singular curves, inside the momentum envelope, consisting of two perpendicular circles described by

$$H_x^2 + H_z^2 = 4 \,(H_y = 0), \qquad H_y^2 + H_z^2 = 4 \,(H_x = 0)$$

Similarly, we can also obtain the 0H singularity surface as shown in Fig. 4. The 0H surface represents a singularity condition where two CMGs are aligned along the desired momentum vector direction and the other two CMGs in the opposite direction. The 0H surface does not necessarily mean a zero total momentum. Only if they are antiparallel does the total momentum become zero. In a composite singularity surface plot, consisting of both the 0H and 4H surfaces, the four trumpetlike funnels of the 0H surface are smoothly patched to the 4H saturation surface along the edges of the circular windows (2H surfaces).

Example 3.3: Pyramid Array with Skew Angle of β

For a typical pyramid configuration of four single-gimbal CMGs with skew angle of β, we have

$$e_1 = \pm\sqrt{1 - (s\beta u_x + c\beta u_z)^2}, \qquad e_2 = \pm\sqrt{1 - (s\beta u_y + c\beta u_z)^2}$$

$$e_3 = \pm\sqrt{1 - (-s\beta u_x + c\beta u_z)^2}$$

$$e_4 = \pm\sqrt{1 - (-s\beta u_y + c\beta u_z)^2}$$

Furthermore, analytic expressions for the singular momentum surfaces, (H_x, H_y, H_z), can be obtained as

$$H_x = \frac{c\beta(-s\beta u_z + c\beta u_x)}{e_1} + \frac{u_x}{e_2} + \frac{c\beta(s\beta u_z + c\beta u_x)}{e_3} + \frac{u_x}{e_4}$$

$$H_y = \frac{u_y}{e_1} - \frac{c\beta(s\beta u_z - c\beta u_y)}{e_2} + \frac{u_y}{e_3} + \frac{c\beta(s\beta u_z + c\beta u_y)}{e_4}$$

$$H_z = \frac{s\beta(-c\beta u_x + s\beta u_z)}{e_1} + \frac{s\beta(s\beta u_z - c\beta u_y)}{e_2} + \frac{s\beta(s\beta u_z + c\beta u_x)}{e_3} + \frac{s\beta(s\beta u_z + c\beta u_y)}{e_4}$$

where $u_x = \sin\theta_2$, $u_y = -\sin\theta_1 \cos\theta_2$, and $u_z = \cos\theta_1 \cos\theta_2$.

Using these expressions, one can obtain 4H, 2H, and 0H singularity surfaces, as presented in Ref. 16. In a composite singularity surface plot, consisting of the 2H and 4H singularity surfaces, the eight trumpetlike funnels of the 2H surface are smoothly patched to the 4H saturation surface along the edges of the circular holes, resulting in the momentum envelope but with eight nonflat windows.

IV. Singularity Analysis Using the Binet–Cauchy Identity

In the previous section, a method developed by Margulies and Auburn[2] was used to analyze and visualize the singular momentum surfaces. A different approach for determining the singular momentum surfaces, called the cutting-plane method, can also be found in the literature.[22] These two techniques do not explicitly require the singular gimbal angle information to determine the singular momentum surfaces.

However, it is often preferred to determine all possible singular gimbal angles 1) to understand and characterize all possible singularities of CMG systems, 2) to be used for a direct singularity-avoidance logic (e.g., Refs. 3 and 7), or 3) to determine singular momentum surfaces indirectly.[16]

Singularity condition (20) can be rewritten in matrix form as

$$\mathbf{A}^T\mathbf{u} = 0 \tag{29}$$

In other words, the singular vector $\mathbf{u}$ of the Jacobian matrix $\mathbf{A}$ is the null space vector of $\mathbf{A}^T$; that is, $\mathbf{u} = \text{null}(\mathbf{A}^T)$. Nontrivial solutions, $\mathbf{u} \neq 0$, exist for $(\mathbf{A}\mathbf{A}^T)\mathbf{u} = 0$ if and only if $\mathbf{A}\mathbf{A}^T$ is singular. That is, we have the singularity condition of the form

$$\det(\mathbf{A}\mathbf{A}^T) = 0 \tag{30}$$

In general, the singularity condition defines a set of surfaces in $\mathbf{x}$ space, or equivalently, in $\mathbf{H}$ space. The simplest singular state is the momentum saturation singularity characterized by the momentum envelope, which is a three-dimensional surface representing the maximum available angular momentum of CMGs along any given direction. Any singular state for which the total CMG momentum vector is inside the momentum envelope is called "internal."

The singularity condition can also be written by using the Binet–Cauchy identity[23] as follows:

$$\det(\mathbf{A}\mathbf{A}^T) \equiv \sum_{i=1}^{n} M_i^2 = 0 \tag{31}$$

where $M_i = \det(\mathbf{A}_i)$ are the Jacobian minors of order 3 and $\mathbf{A}_i = \mathbf{A}$ with the ith column removed.

Singularity conditions (31) for the pyramid array of four single-gimbal CMGs become

$$M_1 = s\beta\big[(s_2s_3c_4 + c_2s_3s_4) + c\beta(c_2c_3s_4 - s_2c_3c_4) + 2(c\beta)^2c_2c_3c_4\big] = 0 \tag{32a}$$

$$M_2 = s\beta\big[(s_3s_4c_1 + c_3s_4s_1) + c\beta(c_3c_4s_1 - s_3c_4c_1) + 2(c\beta)^2c_3c_4c_1\big] = 0 \tag{32b}$$

$$M_3 = s\beta\big[(s_4s_1c_2 + c_4s_1s_2) + c\beta(c_4c_1s_2 - s_4c_1c_2) + 2(c\beta)^2c_4c_1c_2\big] = 0 \tag{32c}$$

$$M_4 = s\beta\big[(s_1s_2c_3 + c_1s_2s_3) + c\beta(c_1c_2s_3 - s_1c_2c_3) + 2(c\beta)^2c_1c_2c_3\big] = 0 \tag{32d}$$

where $s_i \equiv \sin x_i$ and $c_i \equiv \cos x_i$. Although these singularity conditions based on the Binet–Cauchy identity have been discussed in the literature (e.g., Refs. 2, 4, and 5), a new approach to computing the singularity momentum surfaces using the singularity conditions $M_i = 0$ is presented here.

Because the minimum rank of the Jacobian matrix $\mathbf{A}$ is 2, the four conditions $M_1 = M_2 = M_3 = M_4 = 0$ are not independent of one another and only two of them are independent. Consequently, any two of these four conditions may be used to find the singular gimbal angles as follows.

When $c_i \neq 0$, the singularity conditions can be simplified as

$$\tan x_3(\tan x_2 + \tan x_4) + c\beta(\tan x_4 - \tan x_2) = -2(c\beta)^2 \tag{33}$$

$$\tan x_4(\tan x_3 + \tan x_1) + c\beta(\tan x_1 - \tan x_3) = -2(c\beta)^2 \tag{34}$$

$$\tan x_1(\tan x_4 + \tan x_2) + c\beta(\tan x_2 - \tan x_4) = -2(c\beta)^2 \tag{35}$$

$$\tan x_2(\tan x_1 + \tan x_3) + c\beta(\tan x_3 - \tan x_1) = -2(c\beta)^2 \tag{36}$$

Because the minimum rank of the Jacobian matrix $\mathbf{A}$ is 2, only two of these four conditions are independent. Therefore, these four equations, Eqs. (33–36), yield six singular gimbal angle combinations.

For example, we have, in case 1, for all (x_1, x_3), determine (x_2, x_4) using Eqs. (34) and (36):

$$x_2 = \tan^{-1}\left[\frac{-2(c\beta)^2 - c\beta\tan x_3 + c\beta\tan x_1}{\tan x_1 + \tan x_3}\right] \tag{37}$$

$$x_4 = \tan^{-1}\left[\frac{-2(c\beta)^2 - c\beta\tan x_1 + c\beta\tan x_3}{\tan x_1 + \tan x_3}\right] \tag{38}$$

The other five cases can be found in Ref. 16.

There are six additional cases when $c_i = 0$ (i.e., $\tan x_i = \pm\infty$). For example, we have

Case 7:

$$\sin(x_2 + x_4) = 0 \quad \text{when} \quad \cos x_1 = \cos x_3 = 0 \tag{39}$$

Case 8:

$$\sin(x_1 + x_3) = 0 \quad \text{when} \quad \cos x_2 = \cos x_4 = 0 \tag{40}$$

and the other four additional cases can be found in Ref. 16.

Singular surfaces in the three-dimensional vector momentum space, $\mathbf{H} = (H_x, H_y, H_z)$, are then defined as surfaces mapped by

$$H_x = -c\beta\sin x_1 - \cos x_2 + c\beta\sin x_3 + \cos x_4 \tag{41a}$$

$$H_y = \cos x_1 - c\beta\sin x_2 - \cos x_3 + c\beta\sin x_4 \tag{41b}$$

$$H_z = s\beta\sin x_1 + s\beta\sin x_2 + s\beta\sin x_3 + s\beta\sin x_4 \tag{41c}$$

As an illustrative example, the singular momentum projection on the (H_x, H_z) plane for case 7 (with $\beta = 54.7$ deg) is shown in Fig. 5. For this case, the singularity conditions become

$$(x_1, x_3) = (\pm\pi/2, \pm\pi/2)$$

$$x_2 + x_4 = 0 \qquad \text{or} \qquad x_2 + x_4 = \pi$$

For $x_2 + x_4 = 0$, there are four line singularities passing through the four points denoted by $*$ as shown in Fig. 5. For $x_2 + x_4 = \pi$, the four ellipses on the (H_x, H_z) plane with $H_y \equiv 0$ can be found:

$$H_x^2 + \frac{(H_z \pm 2\sin\beta)^2}{\sin^2\beta} = 4, \qquad (H_x \pm 2\cos\beta)^2 + \frac{H_z^2}{\sin^2\beta} = 4$$

Detailed results for computing all possible singular gimbal angles and also visualizing the singular momentum surfaces using this new approach can be found in Ref. 16. The proposed method provides detailed information about singular gimbal angles and their direct relationships to the resulting singular momentum surfaces. It also provides a systematic way of determining all possible singular gimbal angles, whereas the method by Margulies and Aubrun[2] does not.

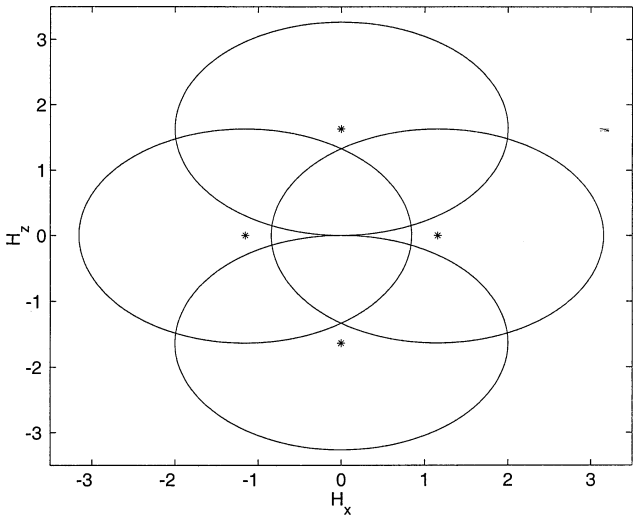

Fig. 5 Singular momentum projection on the (H_x, H_z) plane for case 7 with $\beta = 54.7$ deg.

V. CMG Null Motions

The so-called null motions of CMGs are defined as CMG gimbal motions that generate no net torque from the CMGs. One of the principal difficulties in using CMGs for spacecraft attitude control and momentum management is the geometric singularity problem in which no control torque is generated for the commanded control torque along a particular direction. At a singularity, CMG torque is available in all but one direction. In practice, the null motions are often employed to avoid and/or escape such a singularity situation.

There are two types of singular states, hyperbolic states and elliptic states.[2] The hyperbolic singular states can sometimes be escaped through null motion whereas the elliptic singular states cannot be escaped through any null motion. Although null motion can be generated at the hyperbolic singularity, the mere existence of null motion does not guarantee escape from the hyperbolic singularity. This so-called degenerate null motion problem was briefly mentioned by Bedrossian et al.[4,5] without any specific example.

In this section, a mathematical framework for analyzing such null motions as well as for determining the singularity types is established by expanding on the previous work by Bedrossian et al.[4,5] This section is also intended to provide the reader with some new physical insights into the null motions (in particular, the degenerate null motions). Several illustrative examples with significant new results are presented.

The virtual momentum vector $\delta \boldsymbol{h}_i$ associated with the ith CMG is defined such that

$$\delta \boldsymbol{H} = \sum_{i=1}^{n} \delta \boldsymbol{h}_i = 0 \tag{42}$$

which is in fact the condition for null motion, also called virtual or zero-torque motion. The virtual momentum vector $\delta \boldsymbol{h}_i$ is different from the actual momentum vector change $d\boldsymbol{h}_i$, but it must be compatible with null motion constraint (42) irrespective of time.

The virtual (null motion) momentum vector $\delta \boldsymbol{h}_i$ can be expanded in a Taylor series as follows:

$$\begin{aligned}\delta \boldsymbol{H} &= \sum_{i=1}^{n} \delta \boldsymbol{h}_i \\ &= \sum_{i=1}^{n} \left(\frac{d\boldsymbol{h}_i}{dx_i}\delta x_i + \frac{1}{2!}\frac{d^2\boldsymbol{h}_i}{dx_i^2}\delta x_i^2 + \frac{1}{3!}\frac{d^3\boldsymbol{h}_i}{dx_i^3}\delta x_i^3 + \cdots \right) \\ &= \sum_{i=1}^{n} \left(\boldsymbol{f}_i \delta x_i - \frac{1}{2!}\boldsymbol{h}_i \delta x_i^2 - \frac{1}{3!}\boldsymbol{f}_i \delta x_i^3 + \cdots \right) = 0 \end{aligned} \tag{43}$$

where δx_i are the virtual (null motion) gimbal angle displacements from arbitrary gimbal angles x_i, and $\boldsymbol{f}_i = d\boldsymbol{h}_i / dx_i$.

The first-order necessary condition for null motion is then given by

$$\sum_{i=1}^{n} \boldsymbol{f}_i \delta x_i = 0 \tag{44}$$

which can be rewritten in matrix form as

$$\sum_{i=1}^{n} \mathbf{f}_i \delta x_i = \mathbf{A}\delta \mathbf{x} = 0 \tag{45}$$

where $\delta \mathbf{x} = (\delta x_1, \ldots, \delta x_n)$ is called the null motion displacement vector and $\mathbf{A}$ is the Jacobian matrix previously defined in Eq. (6). In other words, the null vector $\delta \mathbf{x}$ is the null-space vector of $\mathbf{A}$; that is, $\delta \mathbf{x} = \mathbf{n} = \text{null}(\mathbf{A})$ and $\mathbf{An} = 0$. A null-space vector can be obtained as follows[2]:

$$\mathbf{n} = (C_1, C_2, C_3, C_4) = \text{Jacobian null vector}$$

$$C_i = (-1)^{i+1} M_i = \text{order 3 Jacobian cofactor}$$

$$M_i = \det(\mathbf{A}_i) = \text{order 3 Jacobian minor}$$

$$\mathbf{A}_i = \mathbf{A} \text{with ith column removed}$$

However, the mere existence of the local null vectors (the first-order necessary condition for null motion) is not sufficient for an escape by null motion from singularity. The second-order necessary condition needs to be checked.

To test whether null motion is possible at a given singularity or to determine its type of singularity (i.e., elliptic or hyperbolic), consider the null motion constraint expressed in matrix form as

$$\begin{aligned}\delta \mathbf{H} &= \mathbf{H}(\mathbf{x} + \delta \mathbf{x}) - \mathbf{H}(\mathbf{x}) \\ &= \sum_{i=1}^{n} \left(\mathbf{f}_i \delta x_i - \frac{1}{2!}\mathbf{h}_i \delta x_i^2 - \frac{1}{3!}\mathbf{f}_i \delta x_i^3 + \cdots \right) \\ &= 0 \end{aligned} \tag{46}$$

which is the equivalent matrix representation of Eq. (43).

Taking the inner product of $\delta \mathbf{H}$ with an arbitrary vector $\mathbf{u}$, we obtain

$$\mathbf{u}^T \delta \mathbf{H} = \mathbf{u}^T \left\{ \sum_{i=1}^{n} \left[\mathbf{f}_i \delta x_i - \frac{1}{2!}\mathbf{h}_i(x_i) \delta x_i^2 - \frac{1}{3!}\mathbf{f}_i \delta x_i^3 + \cdots \right] \right\} = 0 \tag{47}$$

Because $\mathbf{u}^T \mathbf{f}_i = 0$ (i = 1, ...,4) when $\mathbf{u}$ is along the singular vector direction, we obtain the constraint equation for null motion as follows:

$$\begin{aligned} 0 &= \mathbf{u}^T \left[\sum_{i=1}^{n} \left(-\frac{1}{2!}\mathbf{h}_i \delta x_i^2 + \frac{1}{4!}\mathbf{h}_i \delta x_i^n + \cdots \right) \right] \\ &= \sum_{i=1}^{n} \left(\mathbf{u}^T \mathbf{h}_i \right) \left(-\frac{1}{2!}\delta x_i^2 + \frac{1}{4!}\delta x_i^n - \cdots \right) \\ &= \sum_{i=1}^{n} e_i (\cos \delta x_i - 1) \end{aligned} \tag{48}$$

where $e_i = \mathbf{u}^T \mathbf{h}_i = \boldsymbol{u} \cdot \boldsymbol{h}_i$, which was previously defined in Sec. III.

Considering only the second-order terms, we obtain the second-order necessary condition for null motion[2,4] as follows:

$$\sum_{i=1}^{n} e_i \delta x_i^2 = 0 \tag{49}$$

which can be rewritten as

$$\delta \mathbf{x}^T \mathbf{E} \delta \mathbf{x} = 0 \tag{50}$$

where $\delta \mathbf{x} = (\delta x_1, \ldots, \delta x_n)$; $\mathbf{E}$ is a diagonal matrix defined as $\mathbf{E} = \text{diag}(e_i)$. If $\mathbf{E}$ is a sign-definite matrix, the only solution to Eq. (50) is $\delta \mathbf{x} = 0$, and null motion is not possible. However, the sign-definiteness of $\mathbf{E}$ is only the sufficient but not necessary condition for the trivial solution, $\delta \mathbf{x} = 0$, to Eq. (50).

The virtual null motion of gimbal angles can be expressed using the first-order necessary condition, as follows[4]:

$$\delta \mathbf{x} = \sum_{i=1}^{n-2} c_i \mathbf{n}_i = \mathbf{N}\mathbf{c} \tag{51}$$

where c_i is the ith weighting coefficient, $\mathbf{c} = (c_1, \ldots, c_{n-2})$, and $\mathbf{n}_i$ are the null-space basis vectors of the Jacobian matrix $\mathbf{A}$ such that $\mathbf{A}\mathbf{n}_i = 0$ or $\mathbf{N} = \text{null}(\mathbf{A})$. Note that at a singularity $\text{rank}(\mathbf{A}) = 2$ and $\text{nullity}(\mathbf{A}) = n - \text{rank}(\mathbf{A})$.

Substituting Eq. (51) into Eq. (50), we obtain the second-order necessary condition of the form[4]:

$$\mathbf{c}^T \mathbf{M} \mathbf{c} = 0 \tag{52}$$

where $\mathbf{M} = \mathbf{N}^T \mathbf{E} \mathbf{N}$.

If $\mathbf{M}$ is a sign-definite matrix, the only solution to Eq. (52) is $\mathbf{c} = 0$, and null motion is not possible. This type of singularity is referred to as an elliptic singularity and, consequently, it cannot be escaped by null motion. The other possibility for $\mathbf{M}$ is to be sign-indefinite (or singular). This type of singularity is referred to as a hyperbolic singularity. As will be illustrated for a system of two single-gimbal CMGs, however, the mere possibility of null motion does not guarantee escape from singularity. Degenerate null motion solutions that do not affect the rank of the Jacobian matrix must be excluded, as discussed in Ref. 4.

Example 5.1: Two Parallel Single-Gimbal CMGs

A system of two parallel single-gimbal CMGs has a Jacobian matrix $\mathbf{A}$ of the form

$$\mathbf{A} = 2 \begin{bmatrix} -\sin\alpha\cos\beta, & -\cos\alpha\sin\beta \\ \cos\alpha\cos\beta, & -\sin\alpha\sin\beta \end{bmatrix} \tag{53}$$

where α is the rotation angle and β the scissor angle, as shown in Fig. 2. The singularity condition becomes

$$|\mathbf{A}| = \sin\beta\cos\beta = 0 \tag{54a}$$

$$\Rightarrow \beta = 0, \pm\pi/2, \pm\pi \ \forall\alpha \tag{54b}$$

The singular momentum surface for $\beta = 0$ is simply a circle of the form $H_x^2 + H_y^2 = 4$. This also confirms the singular momentum surface expression, Eq. (6), previously found directly without recourse to singular gimbal angles. An internal antiparallel 0H singularity for $\beta = \pm\pi/2$ is located at the origin: $(H_x, H_y) = (0, 0)$.

For the 0H singularity at $\mathbf{x} = (\alpha, \beta) = (0, \pi/2)$, illustrated in Fig. 2, the Jacobian matrix becomes

$$\mathbf{A} = \begin{bmatrix} 0 & -2 \\ 0 & 0 \end{bmatrix}$$

with its singular vector of $\mathbf{u} = (0, 1)$, that is, $\mathbf{A}^T\mathbf{u} = 0$. A null-space vector of $\mathbf{A}$ such that $\mathbf{A}\dot{\mathbf{x}} = 0$ is $\dot{\mathbf{x}} = \text{null}(\mathbf{A}) = (1, 0)$. This 0H (antiparallel) singularity has the following null motion constraint:

$$0 = \sum_{i=1}^{2} e_i(\cos\delta x_i - 1) = \cos\delta x_1 - \cos\delta x_2 \tag{55}$$

Its null motion solution is $\delta x_1 = \delta x_2 =$ arbitrary, which corresponds to $\beta = \pi/2$ for any α. This type of singularity with possible null motion is referred to as a hyperbolic singularity. However, this hyperbolic singularity cannot be escaped by null motion, because the singular configuration ($\beta = \pi/2$) remains undisturbed during null motion along the null manifold (or a degenerate null trajectory), as illustrated in Fig. 6. This example demonstrates that the mere existence of null motion does not guarantee escape from a hyperbolic singularity.

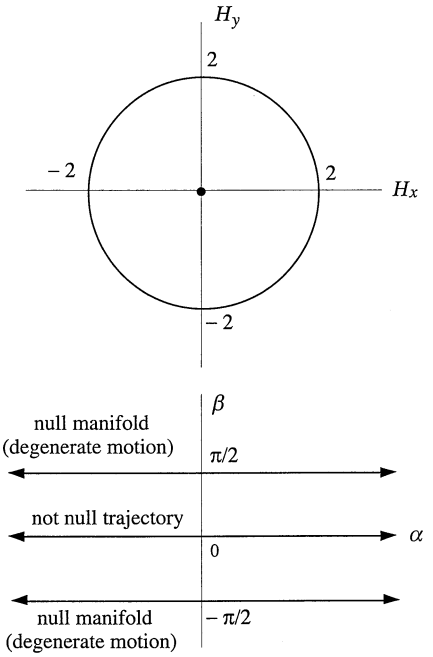

Fig. 6 The (α, β) trajectories for two parallel single-gimbal CMGs.

For the 2H saturation singularity with $\mathbf{x} = (\alpha, \beta) = (0, 0)$, the Jacobian matrix becomes

$$\mathbf{A} = \begin{bmatrix} 0 & 0 \\ 2 & 0 \end{bmatrix}$$

with its singular vector of $\mathbf{u} = (-1, 0)$, that is, $\mathbf{A}^T\mathbf{u} = 0$. Its null-space vector is $\dot{\mathbf{x}} = \text{null}(\mathbf{A}) = (0, 1)$. This saturation singularity has the null motion constraint

$$0 = \sum_{i=1}^{2} e_i(\cos\delta x_i - 1) = \cos\delta x_1 + \cos\delta x_2 - 2 \tag{56}$$

The only solution to this equation is $\delta x_1 = \delta x_2 = 0$; that is, null motion does not exist. This type of singularity with no possible null motion is referred to as an elliptic singularity. All saturation (external) singularities are elliptic; that is, they cannot be escaped by null motion.

Example 5.2: Pyramid Array of Four CMGs

Consider a pyramid array of four CMGs with $\beta = 53.13$ deg. It can be shown that a set of gimbal angles, $\mathbf{x} = (-\pi/2, 0, \pi/2, 0)$, shown in Fig. 7a is an internal elliptic singularity with its singular vector of $\mathbf{u} = (1, 0, 0)$, as follows:

$$\mathbf{A} = \begin{bmatrix} 0 & 0 & 0 & 0 \\ 1 & -0.6 & 1 & 0.6 \\ 0 & 0.8 & 0 & 0.8 \end{bmatrix}$$

$$\text{null}(\mathbf{A}) = \mathbf{N} = \begin{bmatrix} -0.7952 & 0 \\ -0.2774 & -0.5392 \\ 0.4623 & -0.6470 \\ 0.2774 & 0.5392 \end{bmatrix}$$

$$\text{null}(\mathbf{A}^T) = \mathbf{u} = [\,1 \quad 0 \quad 0\,]^T$$

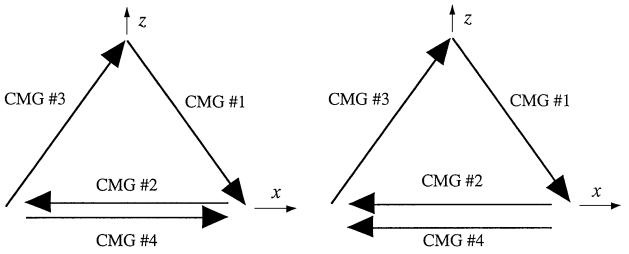

a) 2H internal elliptic singularity b) 0H internal hyperbolic singularity

Fig. 7 Singularity illustration for a pyramid mounting arrangement of four single-gimbal CMGs.

$$\mathbf{E} = \text{diag}\left(\mathbf{u}^T \mathbf{h}_i\right) = \text{diag}(0.6, -1.0, 0.6, 1.0)$$

$$\mathbf{M} = \mathbf{N}^T \mathbf{E} \mathbf{N} = \begin{bmatrix} 0.5077 & -0.1795 \\ -0.1795 & 0.2512 \end{bmatrix}$$

$$\text{eig}(\mathbf{M}) = 0.1588, 0.6$$

However, a set of gimbal angles, $\mathbf{x} = (-\pi/2, 0, \pi/2, \pi)$, shown in Fig. 7b can be shown to be a hyperbolic singularity with its singular vector of $\mathbf{u} = (1, 0, 0)$. It can be further shown that this hyperbolic singularity can be escaped by null motion because its null motion is not a degenerate solution.[4]

Example 5.3: Three Parallel Single-Gimbal CMGs

For a system of three single-gimbal CMGs with parallel gimbal axes, described by Eqs. (14) and (15), the singularity condition becomes

$$\begin{aligned} \det(\mathbf{A}\mathbf{A}^T) &= M_1^2 + M_2^2 + M_3^2 \\ &= \sin^2(x_3 - x_2) + \sin^2(x_3 - x_1) + \sin^2(x_2 - x_1) \\ &= 0 \end{aligned} \tag{57}$$

and singular gimbal angles can be found as

$$x_1 = x_2 = x_3 \text{ (external 3H singularity)}$$

$$x_i = x_j, x_k = x_i \pm \pi \text{ (internal 1H singularity)}$$

The singular momentum surfaces are then simply described by two circles, as shown in Fig. 8. The internal antiparallel (1H) singularity and the external parallel (3H) singularity are also illustrated in Fig. 8.

The 1H singularity has the null motion constraint

$$\begin{aligned} 0 &= \sum_{i=1}^{3} e_i(\cos \delta x_i - 1) \\ &= (\cos \delta x_1 - 1) + (\cos \delta x_2 - 1) - (\cos \delta x_3 - 1) \\ &= \cos \delta x_1 + \cos \delta x_2 - \cos \delta x_3 - 1 \end{aligned} \tag{58}$$

Its nondegenerate null motion solution can be found as $\delta x_2 = \delta x_3$ and $\delta x_1 = 0$ and, thus, it is a hyperbolic singularity that can be escaped by null motion.

A new set of orthogonal coordinates (x, y, z) for gimbal angles, described by Margulies and Aubrun (but not explicitly provided in Ref. 2), can be found as

$$\begin{bmatrix} x \\ y \\ z \end{bmatrix} = \begin{bmatrix} 1/\sqrt{2} & -1/\sqrt{2} & 0 \\ 1/\sqrt{6} & 1/\sqrt{6} & -2/\sqrt{6} \\ 1/\sqrt{3} & 1/\sqrt{3} & 1/\sqrt{3} \end{bmatrix} \begin{bmatrix} x_1 \\ x_2 \\ x_3 \end{bmatrix} \tag{59}$$

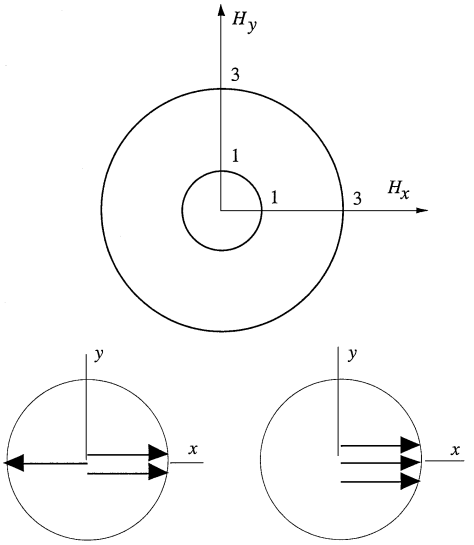

a) 1H antiparallel singularity b) 3H parallel singularity

Fig. 8 Singularity illustration for three single-gimbal CMGs with parallel gimbal axes.

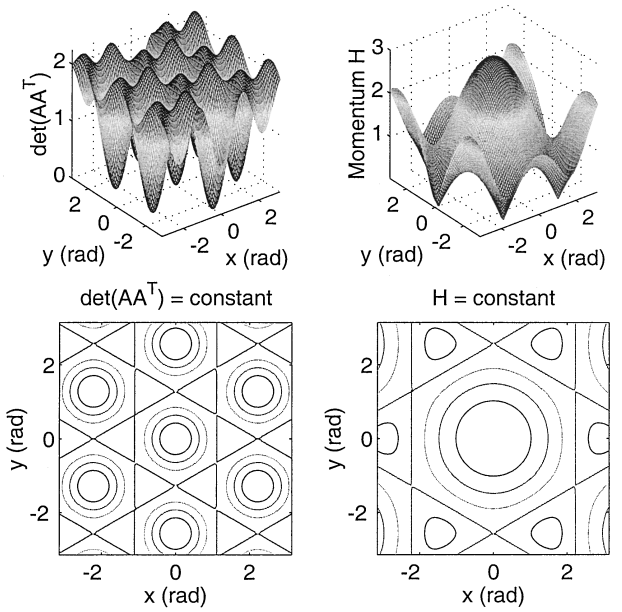

Fig. 9 Contour plots of $\det(\mathbf{A}\mathbf{A}^T)$ and H for a system of three parallel CMGs. Note that (x, y) are the new transformed gimbal angle coordinates defined by Eq. (59).

or

$$\begin{bmatrix} x_1 \\ x_2 \\ x_3 \end{bmatrix} = \begin{bmatrix} 1/\sqrt{2} & 1/\sqrt{6} & 1/\sqrt{3} \\ -1/\sqrt{2} & 1/\sqrt{6} & 1/\sqrt{3} \\ 0 & -2/\sqrt{6} & 1/\sqrt{3} \end{bmatrix} \begin{bmatrix} x \\ y \\ z \end{bmatrix} \tag{60}$$

Using Eq. (60), we can then express $\det(\mathbf{A}\mathbf{A}^T)$ and the total angular momentum H as[2]

$$\det(\mathbf{A}\mathbf{A}^T) = 2 - \cos^2 \frac{2x}{\sqrt{2}} - \cos \frac{2x}{\sqrt{2}} \cos \frac{6y}{\sqrt{6}} \tag{61a}$$

$$H^2 = 1 + 4\cos^2 \frac{x}{\sqrt{2}} + 4\cos \frac{x}{\sqrt{2}} \cos \frac{3y}{\sqrt{6}} \tag{61b}$$

which are independent of z.

Contour plots of $\det(\mathbf{A}\mathbf{A}^T)$ and H vs (x, y) are shown in Fig. 9. In the contour plot of H, one can easily identify an elliptic

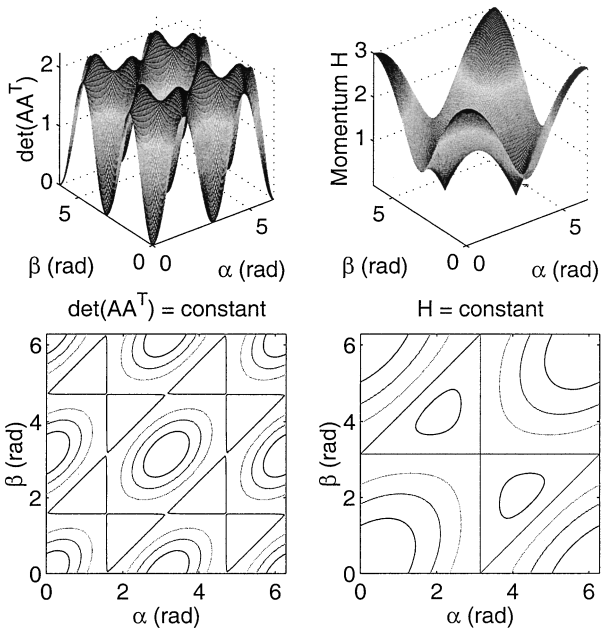

Fig. 10 Contour plots of $\det(\mathbf{AA}^T)$ and H vs (α, β) for a system of three parallel CMGs.

singularity at the center and hyperbolic singularities at the six saddlelike points. The constant-H lines of $H = 1$ connecting the internal hyperbolic singularities are null motion trajectories. The zero-momentum points are not singular points.

Instead of employing (x, y, z) introduced by Margulies and Aubrun, we may introduce two angles (α, β) as

$$\alpha = x_2 - x_1 \tag{62a}$$

$$\beta = x_3 - x_1 \tag{62b}$$

Then we simply obtain

$$\det(\mathbf{AA}^T) = \sin^2\alpha + \sin^2(\alpha - \beta) + \sin^2\beta \tag{63}$$

$$H^2 = (1 + \cos\alpha + \cos\beta)^2 + (\sin\alpha + \sin\beta)^2 \tag{64}$$

Contour plots of $\det(\mathbf{AA}^T)$ and H vs (α, β) are also shown in Fig. 10. The external elliptic singularities, internal hyperbolic singularities, and null motion manifolds can also be easily identified in the contour plot of H in Fig. 10.

VI. Surface Theory of Differential Geometry

In this section, the singularity surface problem is further examined by applying the surface theory of differential geometry.[24,25] This subject is certainly mathematical in nature; however, it is also of practical importance for a better understanding of CMG systems and also even for developing CMG steering laws, as attempted by many previous researchers, including Margulies and Aubrun.[2]

One can analyze, compute, and visualize the singular surfaces without employing the differential surface theory, as demonstrated in the preceding sections. However, this section is intended to provide the reader with the basic mathematical foundation of the theory of differential geometry as it is applied to the geometric theory of CMG systems. Further study is necessary to fully exploit the differential surface geometry theory, and this section will certainly help the reader further advance in this subject.

Let a unit vector along all possible directions in three-dimensional space (except along the gimbal-axis directions) be parameterized as

$$\begin{aligned}\boldsymbol{u} &= u_x\boldsymbol{i} + u_y\boldsymbol{j} + u_z\boldsymbol{k} \\ &= \sin\theta_2\boldsymbol{i} - \sin\theta_1\cos\theta_2\boldsymbol{j} + \cos\theta_1\cos\theta_2\boldsymbol{k}\end{aligned} \tag{65}$$

which was previously introduced in Eq. (17). Then, we obtain the differential of $\boldsymbol{u}$ as

$$d\boldsymbol{u} = \boldsymbol{u}_1 d\theta_1 + \boldsymbol{u}_2 d\theta_2 \tag{66}$$

where

$$\boldsymbol{u}_1 \equiv \frac{\partial \boldsymbol{u}}{\partial\theta_1} = -\cos\theta_1\cos\theta_2\boldsymbol{j} - \sin\theta_1\cos\theta_2\boldsymbol{k}$$

$$\boldsymbol{u}_2 \equiv \frac{\partial \boldsymbol{u}}{\partial\theta_2} = \cos\theta_2\boldsymbol{i} + \sin\theta_1\sin\theta_2\boldsymbol{j} - \cos\theta_1\sin\theta_2\boldsymbol{k}$$

Note that $|\boldsymbol{u}_1| = \cos^2\theta_2$, $|\boldsymbol{u}_2| = 1$, and $\boldsymbol{u}_1 \cdot \boldsymbol{u}_2 = 0$.

Similarly, the differential of the singular momentum vector or singularity surface vector $\boldsymbol{H}(\theta_1, \theta_2)$ can also be represented as

$$d\boldsymbol{H} = \frac{\partial \boldsymbol{H}}{\partial\theta_1}d\theta_1 + \frac{\partial \boldsymbol{H}}{\partial\theta_2}d\theta_2 = \boldsymbol{H}_1 d\theta_1 + \boldsymbol{H}_2 d\theta_2 \tag{67}$$

where

$$\boldsymbol{H}_i \equiv \frac{\partial \boldsymbol{H}}{\partial\theta_i} = \frac{\partial H_x}{\partial\theta_i}\boldsymbol{i} + \frac{\partial H_y}{\partial\theta_i}\boldsymbol{j} + \frac{\partial H_z}{\partial\theta_i}\boldsymbol{k}$$

The *first fundamental form* of the singularity surface vector $\boldsymbol{H}$ is given by

$$\begin{aligned}\mathrm{I} &\equiv d\boldsymbol{H}\cdot d\boldsymbol{H} = (\boldsymbol{H}_1 d\theta_1 + \boldsymbol{H}_2 d\theta_2)\cdot(\boldsymbol{H}_1 d\theta_1 + \boldsymbol{H}_2 d\theta_2) \\ &= \sum_{i,j=1}^{2} G_{ij} d\theta_i d\theta_j = d\boldsymbol{\theta}^T \mathbf{G} d\boldsymbol{\theta} \\ &= [\,d\theta_1 \quad d\theta_2\,]\begin{bmatrix} G_{11} & G_{12} \\ G_{12} & G_{22}\end{bmatrix}\begin{bmatrix} d\theta_1 \\ d\theta_2\end{bmatrix}\end{aligned} \tag{68}$$

where $d\boldsymbol{\theta} = (d\theta_1, d\theta_2)$, $\mathbf{G} = [G_{ij}] = \mathbf{G}^T > 0$, and

$$G_{ij} \equiv \boldsymbol{H}_i \cdot \boldsymbol{H}_j = \frac{\partial H_x}{\partial\theta_i}\frac{\partial H_x}{\partial\theta_j} + \frac{\partial H_y}{\partial\theta_i}\frac{\partial H_y}{\partial\theta_j} + \frac{\partial H_z}{\partial\theta_i}\frac{\partial H_z}{\partial\theta_j}$$

In this paper, we will employ the following vector/matrix dot-product operation:

$$\begin{bmatrix}\boldsymbol{H}_1 \\ \boldsymbol{H}_2\end{bmatrix}\cdot\begin{bmatrix}\boldsymbol{H}_1 & \boldsymbol{H}_2\end{bmatrix} \equiv \begin{bmatrix}\boldsymbol{H}_1\cdot\boldsymbol{H}_1 & \boldsymbol{H}_1\cdot\boldsymbol{H}_2 \\ \boldsymbol{H}_2\cdot\boldsymbol{H}_1 & \boldsymbol{H}_2\cdot\boldsymbol{H}_2\end{bmatrix} = \mathbf{G} \tag{69}$$

The square of an element of arc length, ds^2, is also often used to denote the first fundamental form of the surface:

$$ds^2 = G_{11}(d\theta_1)^2 + 2G_{12}d\theta_1 d\theta_2 + G_{22}(d\theta_2)^2 \tag{70}$$

and G_{ij} are the components of the so-called metric tensor or fundamental tensor of the two-dimensional Riemannian geometry. The first fundamental form enables us to measure lengths, angles, and areas in a surface.

The *second fundamental form* of the singularity surface vector $\boldsymbol{H}$ is given by

$$\begin{aligned}\mathrm{II} &\equiv -d\boldsymbol{H}\cdot d\boldsymbol{u} = -(\boldsymbol{H}_1 d\theta_1 + \boldsymbol{H}_2 d\theta_2)\cdot(\boldsymbol{u}_1 d\theta_1 + \boldsymbol{u}_2 d\theta_2) \\ &= \sum_{i,j=1}^{2} B_{ij} d\theta_i d\theta_j = d\boldsymbol{\theta}^T \mathbf{B} d\boldsymbol{\theta} \\ &= [\,d\theta_1 \quad d\theta_2\,]\begin{bmatrix} B_{11} & B_{12} \\ B_{21} & B_{22}\end{bmatrix}\begin{bmatrix} d\theta_1 \\ d\theta_2\end{bmatrix}\end{aligned} \tag{71}$$

where $B_{ij} \equiv -\boldsymbol{H}_i \cdot \boldsymbol{u}_j$.

Differentiating the orthogonality relation, $\boldsymbol{H}_i \cdot \boldsymbol{u} = 0$, we obtain

$$\boldsymbol{H}_{ij} \cdot \boldsymbol{u} + \boldsymbol{H}_i \cdot \boldsymbol{u}_j = 0 \tag{72}$$

where $\boldsymbol{H}_{ij} \equiv \partial^2 \boldsymbol{H}/\partial\theta_i \partial\theta_j$. Consequently, we have

$$B_{ij} \equiv -\boldsymbol{H}_i \cdot \boldsymbol{u}_j = \boldsymbol{H}_{ij} \cdot \boldsymbol{u} \tag{73}$$

and $\mathbf{B} = \mathbf{B}^T$ since $\boldsymbol{H}_{ij} = \boldsymbol{H}_{ji}$.

The *third fundamental form* of the surface is given by

$$\begin{aligned} \text{III} &\equiv d\boldsymbol{u} \cdot d\boldsymbol{u} = (\boldsymbol{u}_1 d\theta_1 + \boldsymbol{u}_2 d\theta_2) \cdot (\boldsymbol{u}_1 d\theta_1 + \boldsymbol{u}_2 d\theta_2) \\ &= \sum_{i,j=1}^{2} C_{ij} d\theta_i d\theta_j = d\boldsymbol{\theta}^T \mathbf{C} d\boldsymbol{\theta} \\ &= [\, d\theta_1 \quad d\theta_2 \,] \begin{bmatrix} C_{11} & C_{12} \\ C_{12} & C_{22} \end{bmatrix} \begin{bmatrix} d\theta_1 \\ d\theta_2 \end{bmatrix} \end{aligned} \tag{74}$$

where $C_{ij} \equiv \boldsymbol{u}_i \cdot \boldsymbol{u}_j$ and $\mathbf{C} = \mathbf{C}^T > 0$.

Defining the so-called Weingarten transformation as

$$\begin{bmatrix} \boldsymbol{u}_1 \\ \boldsymbol{u}_2 \end{bmatrix} = -\begin{bmatrix} D_{11} & D_{12} \\ D_{21} & D_{22} \end{bmatrix} \begin{bmatrix} \boldsymbol{H}_1 \\ \boldsymbol{H}_2 \end{bmatrix} = -\mathbf{D} \begin{bmatrix} \boldsymbol{H}_1 \\ \boldsymbol{H}_2 \end{bmatrix} \tag{75}$$

we simply obtain

$$\begin{aligned} \mathbf{B} &\equiv -\begin{bmatrix} \boldsymbol{H}_1 \\ \boldsymbol{H}_2 \end{bmatrix} \cdot [\, \boldsymbol{u}_1 \quad \boldsymbol{u}_2 \,] \\ &= \begin{bmatrix} \boldsymbol{H}_1 \\ \boldsymbol{H}_2 \end{bmatrix} \cdot [\, \boldsymbol{H}_1 \quad \boldsymbol{H}_2 \,] \mathbf{D}^T = \mathbf{G}\mathbf{D}^T \end{aligned} \tag{76}$$

The Weingarten transformation matrix is then obtained as

$$\mathbf{D} = \mathbf{G}^{-1}\mathbf{B} = \mathbf{B}\mathbf{G}^{-1} \tag{77}$$

and $\mathbf{D} = \mathbf{D}^T$. We also have

$$\begin{aligned} \mathbf{C} &\equiv \begin{bmatrix} \boldsymbol{u}_1 \\ \boldsymbol{u}_2 \end{bmatrix} \cdot \begin{bmatrix} \boldsymbol{u}_1 & \boldsymbol{u}_2 \end{bmatrix} = \mathbf{D} \begin{bmatrix} \boldsymbol{H}_1 \\ \boldsymbol{H}_2 \end{bmatrix} \cdot [\, \boldsymbol{H}_1 \quad \boldsymbol{H}_2 \,] \mathbf{D}^T \\ &= \mathbf{D}\mathbf{G}\mathbf{D}^T = \mathbf{D}\mathbf{B} = \mathbf{G}^{-1}\mathbf{B}^2 = \mathbf{B}^2\mathbf{G}^{-1} \end{aligned} \tag{78}$$

Similar to the Weingarten transformation, consider a *congruence transformation* of the form

$$\begin{bmatrix} d\theta_1 \\ d\theta_2 \end{bmatrix} = \begin{bmatrix} E_{11} & E_{12} \\ E_{21} & E_{22} \end{bmatrix} \begin{bmatrix} \omega_1 \\ \omega_2 \end{bmatrix} \tag{79}$$

or $d\boldsymbol{\theta} = \mathbf{E}\boldsymbol{\omega}$ where $\mathbf{E} = [E_{ij}]$ is a nonsingular matrix, that diagonalizes the first fundamental form as

$$\begin{aligned} \text{I} &\equiv d\boldsymbol{H} \cdot d\boldsymbol{H} = d\boldsymbol{\theta}^T \mathbf{G} d\boldsymbol{\theta} = \boldsymbol{\omega}^T \mathbf{E}^T \mathbf{G} \mathbf{E} \boldsymbol{\omega} \\ &= \boldsymbol{\omega}^T \mathbf{I} \boldsymbol{\omega} = \omega_1^2 + \omega_2^2 \end{aligned} \tag{80}$$

where $\mathbf{I}$ is an identity matrix. The differential form $d\boldsymbol{H}$ can then be simply written in terms of the linear differential forms, ω_1 and ω_2, as

$$d\boldsymbol{H} = \omega_1 \boldsymbol{e}_1 + \omega_2 \boldsymbol{e}_2 \tag{81}$$

where $\boldsymbol{e}_1$ and $\boldsymbol{e}_2$ are orthogonal unit vectors; that is, $\boldsymbol{e}_i \cdot \boldsymbol{e}_j = \delta_{ij}$.

By applying the congruence transformation, $d\boldsymbol{\theta} = \mathbf{E}\boldsymbol{\omega}$, we rewrite the second fundamental form as

$$\begin{aligned} \text{II} &\equiv -d\boldsymbol{H} \cdot d\boldsymbol{u} = d\boldsymbol{\theta}^T \mathbf{B} d\boldsymbol{\theta} = \boldsymbol{\omega}^T \mathbf{E}^T \mathbf{B} \mathbf{E} \boldsymbol{\omega} = \boldsymbol{\omega}^T \mathbf{L} \boldsymbol{\omega} \\ &= [\, \omega_1 \;\; \omega_2 \,] \begin{bmatrix} L_{11} & L_{12} \\ L_{12} & L_{22} \end{bmatrix} \begin{bmatrix} \omega_1 \\ \omega_2 \end{bmatrix} \end{aligned} \tag{82}$$

where $\mathbf{L} \equiv \mathbf{E}^T \mathbf{B} \mathbf{E}$ is known as the Weingarten mapping matrix in the theory of differential geometry. According to Sylvester's law of inertia, the signs of the eigenvalues of $\mathbf{B}$ are preserved by a congruence transformation since $\det \mathbf{L} = \det \mathbf{B} (\det \mathbf{E})^2$. Note that the symmetry of $\mathbf{B}$ is also preserved by a congruence transformation; that is, $\mathbf{L} = \mathbf{L}^T$.

Furthermore, the second fundamental form can be diagonalized as

$$\begin{aligned} \text{II} &\equiv -d\boldsymbol{H} \cdot d\boldsymbol{u} = [\, \omega_1 \quad \omega_2 \,] \begin{bmatrix} L_{11} & L_{12} \\ L_{12} & L_{22} \end{bmatrix} \begin{bmatrix} \omega_1 \\ \omega_2 \end{bmatrix} \\ &= [\, \omega_1' \quad \omega_2' \,] \boldsymbol{\Phi}^T \mathbf{L} \boldsymbol{\Phi} \begin{bmatrix} \omega_1' \\ \omega_2' \end{bmatrix} \\ &= [\, \omega_1' \quad \omega_2' \,] \begin{bmatrix} k_1 & 0 \\ 0 & k_2 \end{bmatrix} \begin{bmatrix} \omega_1' \\ \omega_2' \end{bmatrix} \end{aligned} \tag{83}$$

where k_1 and k_2 are the eigenvalues of $\mathbf{L}$, and $\boldsymbol{\Phi}$ is a similarity transformation matrix defined as

$$d\boldsymbol{H} = \omega_1 \boldsymbol{e}_1 + \omega_2 \boldsymbol{e}_2 = \omega_1' \boldsymbol{e}_{1'} + \omega_2' \boldsymbol{e}_{2'} \tag{84}$$

where

$$\begin{bmatrix} \boldsymbol{e}_1 \\ \boldsymbol{e}_2 \end{bmatrix} = \begin{bmatrix} \cos\phi & -\sin\phi \\ \sin\phi & \cos\phi \end{bmatrix} \begin{bmatrix} \boldsymbol{e}_{1'} \\ \boldsymbol{e}_{2'} \end{bmatrix} = \boldsymbol{\Phi} \begin{bmatrix} \boldsymbol{e}_{1'} \\ \boldsymbol{e}_{2'} \end{bmatrix}$$

$$\begin{bmatrix} \omega_1 \\ \omega_2 \end{bmatrix} = \begin{bmatrix} \cos\phi & -\sin\phi \\ \sin\phi & \cos\phi \end{bmatrix} \begin{bmatrix} \omega_1' \\ \omega_2' \end{bmatrix} = \boldsymbol{\Phi} \begin{bmatrix} \omega_1' \\ \omega_2' \end{bmatrix}$$

$$\tan 2\phi = \frac{2L_{12}}{L_{11} - L_{22}} \tag{85}$$

Note that $\boldsymbol{\Phi}$ is an orthonormal matrix with $\boldsymbol{\Phi}^T = \boldsymbol{\Phi}^{-1}$ and $\det \boldsymbol{\Phi} = 1$; that is, $\boldsymbol{\Phi}$ is a rotation matrix for $\boldsymbol{\Phi}^T \mathbf{L} \boldsymbol{\Phi} = \text{diag}\{k_1, k_2\}$, and $\det \mathbf{L} = L_{11}L_{22} - L_{12}^2 = k_1 k_2$.

The normal curvature k_n, Gauss curvature k, and mean curvature $\tilde{k}$ are then defined as

$$k_n = k_1 \cos^2\phi + k_2 \sin^2\phi \equiv \text{II}/\text{I} \tag{86a}$$

$$k = k_1 k_2 = \det \mathbf{L} = L_{11}L_{22} - L_{12}^2 \tag{86b}$$

$$\tilde{k} = \tfrac{1}{2}(k_1 + k_2) = \tfrac{1}{2} \text{ tr } \mathbf{L} = \tfrac{1}{2}(L_{11} + L_{22}) \tag{86c}$$

The principal curvatures, k_1 and k_2, are the roots of the following characteristic equation:

$$\det(\mathbf{L} - \lambda \mathbf{I}) = 0 \qquad \text{or} \qquad \det(\mathbf{B} - \lambda \mathbf{G}) = 0 \tag{87}$$

Furthermore, we have the following relationship from Refs. 24 and 25:

$$k\text{I} - 2\tilde{k}\text{II} + \text{III} = 0 \tag{88}$$

where $\text{I} = \boldsymbol{\omega}^T \mathbf{I} \boldsymbol{\omega}$, $\text{II} = \boldsymbol{\omega}^T \mathbf{L} \boldsymbol{\omega}$, and $\text{III} = \boldsymbol{\omega}^T \mathbf{L}^2 \boldsymbol{\omega}$. Equivalently, we have

$$k\mathbf{G} - 2\tilde{k}\mathbf{B} + \mathbf{C} = 0 \tag{89}$$

For the known surfaces, the angle ψ between the parameter lines, the unit normal vector $\boldsymbol{u}$, and B_{ij} can be obtained from the following relationships:

$$\cos\psi = \frac{\boldsymbol{H}_1 \cdot \boldsymbol{H}_2}{|\boldsymbol{H}_1||\boldsymbol{H}_2|} = \frac{G_{12}}{\sqrt{G_{11}G_{22}}} \tag{90a}$$

$$\boldsymbol{u} = \frac{\boldsymbol{H}_1 \times \boldsymbol{H}_2}{|\boldsymbol{H}_1 \times \boldsymbol{H}_2|} = \frac{\boldsymbol{H}_1 \times \boldsymbol{H}_2}{\sqrt{\det \mathbf{G}}} \tag{90b}$$

$$B_{ij} \equiv -\boldsymbol{H}_i \cdot \boldsymbol{u}_j = \boldsymbol{H}_{ij} \cdot \boldsymbol{u} = \frac{\boldsymbol{H}_{ij} \cdot \boldsymbol{H}_1 \times \boldsymbol{H}_2}{\sqrt{\det \mathbf{G}}} \tag{90c}$$

Note that $\det \mathbf{G} > 0$ because $\mathbf{G}$ is a positive-definite matrix.

Taking the differential of the orthogonality condition, $d\boldsymbol{H}\cdot\boldsymbol{u}=0$, we obtain

$$d^2\boldsymbol{H}\cdot\boldsymbol{u}+d\boldsymbol{H}\cdot d\boldsymbol{u}=0 \tag{91}$$

and the second fundamental form can then be written as

$$\mathrm{II}\equiv d^2\boldsymbol{H}\cdot\boldsymbol{u}=\frac{d^2\boldsymbol{H}\cdot\boldsymbol{H}_1\times\boldsymbol{H}_2}{\sqrt{\det\mathbf{G}}} \tag{92}$$

where

$$d^2\boldsymbol{H}\equiv\frac{\partial^2\boldsymbol{H}}{\partial\theta_1^2}(d\theta_1)^2+\frac{\partial^2\boldsymbol{H}}{\partial\theta_1\partial\theta_2}d\theta_1d\theta_2+\frac{\partial^2\boldsymbol{H}}{\partial\theta_2^2}(d\theta_2)^2 \tag{93}$$

Using dyadic notation, we may rewrite singular momentum vector (25) as

$$\boldsymbol{H}=\boldsymbol{H}(\boldsymbol{u})=\sum_{i=1}^{n}\frac{1}{e_i}(\hat{I}-\boldsymbol{g}_i\boldsymbol{g}_i)\cdot\boldsymbol{u} \tag{94}$$

where $\hat{I}$ is a unit dyadic and $e_i=\boldsymbol{h}_i\cdot\boldsymbol{u}=\pm|\boldsymbol{g}_i\times\boldsymbol{u}|$. The differential of the singular momentum vector is then written as[2]

$$d\boldsymbol{H}=\hat{J}\cdot d\boldsymbol{u} \tag{95}$$

where

$$\hat{J}=\sum_{i=1}^{n}\frac{1}{e_i}\boldsymbol{f}_i\boldsymbol{f}_i \tag{96}$$

Since $\boldsymbol{f}_i\cdot\boldsymbol{u}=0$ at singularity, we have $\hat{J}\cdot\boldsymbol{u}=0$. Thus, it is said that $\hat{J}$ is singular of rank 2 and is a symmetric planar dyadic in the tangent plane orthogonal to $\boldsymbol{u}$.

Representing the symmetric planar dyadic $\hat{J}$ as

$$\hat{J}=[\,\boldsymbol{u}_1\quad\boldsymbol{u}_2\,]\begin{bmatrix}J_{11}&J_{12}\\J_{12}&J_{22}\end{bmatrix}\begin{bmatrix}\boldsymbol{u}_1\\\boldsymbol{u}_2\end{bmatrix}=\sum_{i,j=1}^{2}J_{ij}\boldsymbol{u}_i\boldsymbol{u}_j \tag{97}$$

where $\boldsymbol{u}_i\equiv\partial\boldsymbol{u}/\partial\theta_i$ and $J_{ij}=\boldsymbol{u}_i\cdot\hat{J}\cdot\boldsymbol{u}_j$, we also obtain the two fundamental forms of the singularity surface as

$$\begin{aligned}\mathrm{I}&\equiv d\boldsymbol{H}\cdot d\boldsymbol{H}=d\boldsymbol{u}\cdot\hat{J}^2\cdot d\boldsymbol{u}\\&=d\boldsymbol{\theta}^T\mathbf{CJCJC}d\boldsymbol{\theta}=d\boldsymbol{\theta}^T\mathbf{G}d\boldsymbol{\theta}\end{aligned} \tag{98}$$

$$\begin{aligned}\mathrm{II}&\equiv-d\boldsymbol{H}\cdot d\boldsymbol{u}=-d\boldsymbol{u}\cdot\hat{J}\cdot d\boldsymbol{u}\\&=-d\boldsymbol{\theta}^T\mathbf{CJC}d\boldsymbol{\theta}=d\boldsymbol{\theta}^T\mathbf{B}d\boldsymbol{\theta}\end{aligned} \tag{99}$$

and we have

$$\mathbf{B}=-\mathbf{CJC} \tag{100a}$$

$$\mathbf{G}=\mathbf{BC}^{-1}\mathbf{B} \tag{100b}$$

Note that the matrix $\mathbf{C}$, which is not an identity matrix in general, is missing in Eq. (13) of Ref. 2.

In summary, we have $\mathbf{E}^T\mathbf{GE}=\mathbf{I}$, $\mathbf{E}^T\mathbf{BE}=\mathbf{L}$, $\mathbf{E}^T\mathbf{CE}=\mathbf{L}^2$, $\mathbf{C}=\mathbf{B}^2\mathbf{G}^{-1}$, and $\mathbf{D}=\mathbf{BG}^{-1}$. Consequently, we obtain

$$\det\mathbf{C}=\frac{\det\mathbf{B}^2}{\det\mathbf{G}} \tag{101a}$$

$$\det\mathbf{D}=\frac{\det\mathbf{B}}{\det\mathbf{G}} \tag{101b}$$

and

$$\begin{aligned}k\equiv k_1k_2&=\det\mathbf{L}=L_{11}L_{22}-L_{12}^2\\&=\det\mathbf{D}=\frac{\det\mathbf{B}}{\det\mathbf{G}}=\frac{B_{11}B_{22}-B_{12}^2}{G_{11}G_{22}-G_{12}^2}\\&=\frac{1}{\det\mathbf{J}}\frac{1}{\det\mathbf{C}}=\frac{1}{J_{11}J_{22}-J_{12}^2}\frac{1}{\det\mathbf{C}}\\&=\frac{1}{\lambda_1\lambda_2}\frac{1}{\det\mathbf{C}}\end{aligned} \tag{102}$$

where λ_1 and λ_2 are the eigenvalues of $\mathbf{J}$ and $\det\mathbf{C}>0$. Finally, we have

$$\begin{aligned}\mathrm{sign}(k)&=\mathrm{sign}(\det\mathbf{L})=\mathrm{sign}(\det\mathbf{D})\\&=\mathrm{sign}(\det\mathbf{B})=\mathrm{sign}(\det\mathbf{J})\end{aligned} \tag{103}$$

The sign of k provides important information about the shape of the surface in the neighborhood of a given point $\boldsymbol{H}^*$. If $k(\boldsymbol{H}^*)>0$, then $\boldsymbol{H}^*$ is an elliptic point of the surface. If $k(\boldsymbol{H}^*)=0$, then $\boldsymbol{H}^*$ is a parabolic point or a planar umblic of the surface. If $k(\boldsymbol{H}^*)<0$, then $\boldsymbol{H}^*$ is a hyperbolic point of the surface. The two local surfaces are said to be *isometric* if and only if they have identical Gauss curvatures. A closed surface always has elliptic points. A line for which the second fundamental form becomes diagonal is a principal direction. A curve, all of whose tangents are in principal directions, is a curvature line. The normal curvature of a curvature line is a principal curvature of the surface.

The inverse mapping problem[2] is to determine a direction $d\boldsymbol{u}$ such that $\hat{J}\cdot d\boldsymbol{u}=d\boldsymbol{H}$ when $d\boldsymbol{H}$ is given. If the tangent direction of the singularity surface is given by

$$d\boldsymbol{H}=\hat{J}\cdot d\boldsymbol{u} \tag{104}$$

where $\boldsymbol{u}$ is an arbitrary vector defined over the singularity surface, then the inverse mapping theorem of Margulies and Aubrun[2] gives

$$d\boldsymbol{u}=k\hat{J}\cdot d\boldsymbol{H} \tag{105}$$

where $k=k(\boldsymbol{u})$ is the Gauss curvature given by

$$k=2\sum_{i,j=1}^{n}\frac{e_ie_j}{[\det(\mathbf{f}_i,\mathbf{f}_j,\mathbf{u})]^2} \tag{106}$$

$e_i\equiv\boldsymbol{h}_i\cdot\boldsymbol{u}$, and $\det[\mathbf{f}_i,\mathbf{f}_j,\mathbf{u}]\equiv\boldsymbol{f}_i\times\boldsymbol{f}_j\cdot\boldsymbol{u}$.

As an example consider the two orthogonal pairs of two parallel single-gimbal CMGs, with its momentum saturation surface shown in Fig. 3. The singular momentum at $(H_x, H_y, H_z)=(0, 0, 4)$ has $\boldsymbol{u}(0,0)=\boldsymbol{k}$ for $\boldsymbol{u}=\sin\theta_2\boldsymbol{i}-\sin\theta_1\cos\theta_2\boldsymbol{j}+\cos\theta_1\cos\theta_2\boldsymbol{k}$, and

$$\boldsymbol{u}_1=-\boldsymbol{j},\ \boldsymbol{u}_2=\boldsymbol{i},\ \boldsymbol{H}_1=-2\boldsymbol{j},\ \boldsymbol{H}_2=2\boldsymbol{i}$$

$$d\boldsymbol{u}=\boldsymbol{u}_1d\theta_1+\boldsymbol{u}_2d\theta_2=-\boldsymbol{j}d\theta_1+\boldsymbol{i}d\theta_2$$

$$d\boldsymbol{H}=\boldsymbol{H}_1d\theta_1+\boldsymbol{H}_2d\theta_2=-2\boldsymbol{j}d\theta_1+2\boldsymbol{i}d\theta_2$$

For this somewhat trivial case, we have

$$\mathbf{G}=\begin{bmatrix}4&0\\0&4\end{bmatrix},\qquad\mathbf{B}=\begin{bmatrix}-2&0\\0&-2\end{bmatrix},\qquad\mathbf{C}=\begin{bmatrix}1&0\\0&1\end{bmatrix}$$

$$\mathbf{D}=\begin{bmatrix}-1/2&0\\0&-1/2\end{bmatrix},\qquad\mathbf{E}=\begin{bmatrix}1/2&0\\0&1/2\end{bmatrix}$$

$$\mathbf{L}=\begin{bmatrix}-1/2&0\\0&-1/2\end{bmatrix},\qquad\mathbf{J}=\begin{bmatrix}2&0\\0&2\end{bmatrix}$$

$$k_1 = k_2 = -\frac{1}{2}, \qquad k = k_1 k_2 = \frac{1}{4}, \qquad \tilde{k} = -\frac{1}{2}$$

The singularity at $(H_x, H_y, H_z) = (0, 0, 4)$ is thus an elliptic point since $k > 0$, which can also be confirmed by the convexity of the momentum saturation surface shown in Fig. 3.

This example was mainly intended to verify some of the mathematical formulas derived in this section. It is not intended to demonstrate any significant practicality of this approach to the CMG singularity problem. Further study is necessary to fully exploit the differential surface geometry theory as applied to the CMG singularity problem.

VII. Conclusions

In this paper, particular emphasis has been placed on characterizing and visualizing the physical as well as mathematical nature of singularities, singular momentum surfaces, and null motions. It is hoped that the comprehensive mathematical treatment as well as several illustrative examples with significant new results presented in this paper can be utilized toward developing a CMG-based attitude control system for future agile imaging satellites.

Acknowledgments

The author would like to thank the four reviewers and the associate editor for their comments and suggestions for significantly improving the quality of this paper. Special thanks also go to Vaios Lappas and Philip Palmer for providing the author with an opportunity to further explore the CMG singularity problem during his sabbatical leave at the Surrey Space Centre, University of Surrey, Guildford, UK.

References

[1]Crenshaw, J., "2-SPEED, a Single-Gimbal Control Moment Gyro Attitude Control System," AIAA Paper 73-895, Aug. 1973.

[2]Margulies, G., and Aubrun, J. N., "Geometric Theory of Single-Gimbal Control Moment Gyro Systems," *Journal of the Astronautical Sciences*, Vol. 26, No. 2, 1978, pp. 159–191.

[3]Cornick, D. E., "Singularity Avoidance Control Laws for Single Gimbal Control Moment Gyros," AIAA Paper 79-1698, Aug. 1979.

[4]Bedrossian, N. S., Paradiso, J., Bergmann, E. V., and Rowell, D., "Redundant Single-Gimbal Control Moment Gyroscope Singularity Analysis," *Journal of Guidance, Control, and Dynamics*, Vol. 13, No. 6, 1990, pp. 1096–1101.

[5]Bedrossian, N. S., Paradiso, J., Bergmann, E. V., and Rowell, D., "Steering Law Design for Redundant Single-Gimbal Control Moment Gyroscopes," *Journal of Guidance, Control, and Dynamics*, Vol. 13, No. 6, 1990, pp. 1083–1089.

[6]Vadali, S. R., Oh, H., and Walker, S., "Preferred Gimbal Angles for Single Gimbal Control Moment Gyroscopes," *Journal of Guidance, Control, and Dynamics*, Vol. 13, No. 6, 1990, pp. 1090–1095.

[7]Paradiso, J. A., "Global Steering of Single Gimballed Control Moment Gyroscopes Using a Direct Search," *Journal of Guidance, Control, and Dynamics*, Vol. 15, No. 5, 1992, pp. 1236–1244.

[8]Schaub, H., and Junkins, J. L., "Singularity Avoidance Using Null Motion and Variable-Speed Control Moment Gyros," *Journal of Guidance, Control, and Dynamics*, Vol. 23, No. 1, 2000, pp. 11–16.

[9]Ford, K. A., and Hall, C. D., "Singular Direction Avoidance Steering for Control Moment Gyros," *Journal of Guidance, Control, and Dynamics*, Vol. 23, No. 4, 2000, pp. 648–656.

[10]Heiberg, C. J., Bailey, D., and Wie, B., "Precision Spacecraft Pointing Using Single-Gimbal Control Moment Gyros with Disturbance," *Journal of Guidance, Control, and Dynamics*, Vol. 23, No. 1, 2000, pp. 77–85.

[11]Wie, B., *Space Vehicle Dynamics and Control*, AIAA Education Series, AIAA, Washington, DC, 1998, Chap. 7.

[12]Wie, B., Heiberg, C., and Bailey, D., "Singularity Robust Steering Logic for Redundant Single-Gimbal Control Moment Gyros," *Journal of Guidance, Control, and Dynamics*, Vol. 24, No. 5, 2001, pp. 865–872.

[13]Wie, B., Bailey, D., and Heiberg, C., "Robust Singularity Avoidance in Satellite Attitude Control," U.S. Patent 6,039,290, March 2000.

[14]Bailey, D., Heiberg, C., and Wie, B., "Continuous Attitude Control That Avoids CMG Array Singularities," U.S. Patent 6,131,056, Oct. 2000.

[15]Wie, B., Heiberg, C., and Bailey, D., "Rapid Multi-Target Acquisition and Pointing Control of Agile Spacecraft," *Journal of Guidance, Control, and Dynamics*, Vol. 25, No. 1, 2002, pp. 96–104.

[16]Dominguez, J., and Wie, B., "Computation and Visualization of Control Moment Gyroscope Singularities," AIAA Paper 2002-4570, Aug. 2002.

[17]Roser, X., and Sghedoni, M., "Control Moment Gyroscopes (CMGs) and Their Application in Future Scientific Missions," *Proceedings of 3rd ESA International Conference on Spacecraft Guidance, Navigation and Control Systems*, ESTEC, Noordwijk, The Netherlands, Nov. 1996, pp. 523–528.

[18]Defendini, A., Lagadec, K., Guay, P., and Griseri, G., "Low Cost CMG-based AOCS Designs," *Proceedings of 4th ESA International Conference on Spacecraft Guidance, Navigation and Control Systems*, ESTEC, Noordwijk, The Netherlands, Oct. 1999, pp. 393–398.

[19]Defendini, A., et al., "A Compact CMG Products for Agile Satellites," *Proceedings of the 5th International ESA Conference on Spacecraft Guidance, Navigation and Control Systems*, ESTEC, Noordwijk, The Netherlands, Oct. 2002.

[20]Girouart, B., Sebbag, I., and Lachiver, J.-M., "Performances of the Pleiades-HR Agile Attitude Control System," *Proceedings of the 5th International ESA Conference on Spacecraft Guidance, Navigation and Control Systems*, ESTEC, Noordwijk, The Netherlands, Oct. 2002.

[21]Lappas, V. J., Steyn, W. H., and Underwood, C. I., "Laboratory Experiments of a Control Moment Gyroscope Cluster for Agile Small Satellites," *Proceedings of the 5th International ESA Conference on Spacecraft Guidance, Navigation and Control Systems*, ESTEC, Noordwijk, The Netherlands, Oct. 2002.

[22]Stocking, G., and Meffe, M., "Momentum Envelope Topology of Single-Gimbal CMG Arrays for Space Vehicle Control," American Astronomical Society, Paper 87-002, Washington, DC, Jan./Feb. 1987.

[23]Gantmacher, F. R., *The Theory of Matrices*, Chelsea, Vol. 1, 1959, pp. 9, 10.

[24]Guggenheimer, H. W., *Differential Geometry*, Dover, New York, 1963.

[25]Kreyszig, E., *Differential Geometry*, Dover, New York, 1991.